

Article type : Regular Article

A systems biology view of wood formation in *Eucalyptus grandis* trees submitted to different potassium and water regimes

Raphael PLOYET¹, Mônica T. VENEZIANO LABATE², Thais REGIANI CATALDI², Mathias CHRISTINA^{3,4}, Marie MOREL¹, Hélène SAN CLEMENTE¹, Marie DENIS^{5,6}, Bénédicte FAVREAU^{5,6}, Mario TOMAZELLO FILHO⁴, Jean-Paul LACLAU^{3,4}, Carlos ALBERTO LABATE², Gilles CHAIX^{4,5,6}, Jacqueline GRIMA-PETTENATI¹ and Fabien MOUNET¹

¹ Laboratoire de Recherche en Sciences Végétales, Université de Toulouse III, CNRS, UPS, 31326 Castanet-Tolosan, France.

² Max Feffer Laboratory for Plant Genetics, Department of Genetics, College of Agriculture “Luiz de Queiroz”, University of São Paulo, Av. Pádua Dias 11, Piracicaba-SP, POBox 09, 13418-900, Brazil

³ CIRAD, UMR ECO&SOLS, F-34398 Montpellier, France;

⁴ University of São Paulo, Luiz de Queiroz College of Agriculture, Department of Forest Resource, Av. Pádua Dias N° 11, Piracicaba, São Paulo, 13418-900, Brazil

⁵ CIRAD, UMR AGAP, 34395 Montpellier, Cedex 9, France

⁶ AGAP, Univ Montpellier, CIRAD, INRA, Montpellier SupAgro, Montpellier, France

Author for correspondence:

Mounet Fabien

Tel: +33534323825

Email: mounet@lrsv.ups-tlse.fr

Received: 10 November 2018

Accepted: 28 February 2019

ORCID:

Jacqueline GRIMA-PETTENATI (0000-0003-4272-9767)

Mathias CHRISTINA (0000-0003-3618-756X)

This article has been accepted for publication and undergone full peer review but has not been through the copyediting, typesetting, pagination and proofreading process, which may lead to differences between this version and the Version of Record. Please cite this article as doi: 10.1111/nph.15802

This article is protected by copyright. All rights reserved.

Summary

- (1) Wood production in fast-growing *Eucalyptus grandis* trees is highly dependent on both potassium (K) fertilization and water availability but the molecular processes underlying wood formation in response to the combined effects of these two limiting factors are still unknown
- (2) *E. grandis* trees were submitted to four combinations of K-fertilization and water supply. Weighted gene co-expression network analysis (WGCNA) and MixOmics-based co-regulation networks were used to integrate xylem transcriptome, metabolome and complex wood traits. Functional characterization of a candidate gene was performed in transgenic *E. grandis* hairy roots.
- (3) This integrated network-based approach enabled us to identify meaningful biological processes and regulators impacted by K-fertilization and/or water limitation. It revealed that modules of co-regulated genes and metabolites strongly correlated to wood complex traits are in the heart of a complex trade-off between biomass production and stress responses. Nested in these modules, potential new cell wall regulators were identified as further confirmed by the functional characterization of *EgMYB137*.
- (4) These findings provide new insights into the regulatory mechanisms of wood formation under stress conditions pointing out both known and new regulators co-opted by K-fertilization and/or water limitation that may potentially promote adaptive wood traits.

Keywords: Systems biology, Co-regulation networks, Omics integration, Drought, Potassium, Xylem, Transcription factors, *Eucalyptus*.

1. Introduction

Wood, or secondary xylem, is formed by the activity of an internal meristem called the vascular cambium, through a complex differentiation process leading to highly specialized xylem cells characterized by thick, lignified secondary cell walls (SCWs) (Plomion *et al.*, 2001). Besides being a renewable source of material for mankind, providing raw material for timber, paper, energy, second generation biofuels as well as for added-value biomaterials (Mizrachi *et al.*, 2012), wood represents a major carbon sink important for climate regulation (Bonan, 2008). The physicochemical properties of wood, which depend mainly on the chemical composition and the structure of secondary cell walls (SCWs), determine wood industrial end-uses (Mansfield, 2009). In xylem, SCWs are made of

approximately 75% of polysaccharides (cellulose and hemicelluloses) and 25% of lignin, a complex hydrophobic phenolic polymer.

The fast-growing eucalypts characterized by their outstanding growth performance, short-rotation time and wide adaptability are the most planted trees worldwide (Hinchee *et al.*, 2009). Eucalypts plantations are mostly established in tropical and subtropical regions where the main environmental constraints are soil nutrients starvation and drought episodes (Gonçalves *et al.*, 1997). In highly weathered tropical soils, potassium (K) is a major limiting factor of tree growth (Laclau *et al.*, 2009; Wright, 2011; Epron *et al.*, 2012). Besides its essential role in a variety of cellular processes, reviewed in Sardans & Peñuelas (2015), K is considered as a key osmolyte for wood formation (Fromm, 2010). K fertilization in K-deficient soils can lead to a dramatic increase in wood biomass production in tree species such as pine (Smethurst *et al.*, 2007), poplar (Wind *et al.*, 2004; Arend *et al.*, 2004) and eucalypts (Laclau *et al.*, 2009). In these conditions, a higher cambial activity is correlated with a peak of K in the cambial zone (Kuhn *et al.*, 1997; Arend *et al.*, 2002; Wind *et al.*, 2004; Langer *et al.*, 2004; Fromm, 2010). K also influences xylem structure likely through its role in turgor-driven elongation of new xylem cells. It has an impact on SCW deposition dynamics as K-starved trees show earlier initiation of SCW deposition than controls (Dunisch *et al.*, 1998; Langer *et al.*, 2002).

In a context of climate change, the intensity and frequency of future drought episodes are likely to increase in tropical and subtropical regions, affecting *Eucalyptus* plantations productivity (Hawkins & Sutton, 2012; IPCC, 2013). Potassium contributes to plant resistance to abiotic stresses, including drought by improving processes like osmotic adjustment, stomatal aperture control, photosynthesis activation, ROS detoxification and phloem loading of photoassimilates (reviewed in Wang *et al.*, 2013). Some studies suggested that K modulates xylem hydraulic conductance, possibly by interacting with pectins in intervessel pits, enhancing tree resistance to drought (Nardini *et al.*, 2010; Jansen *et al.*, 2011). Recently, using a large-scale through-fall exclusion experiment, Battie-Laclau *et al.* (2016) showed that K fertilization improved water use efficiency and biomass production in *Eucalyptus*. However, during drought episodes, these authors noticed that the beneficial effect of K may not be sufficient to counterbalance the detrimental effect of increased water demand caused by higher growth rates of K-fertilized trees (Battie-Laclau *et al.*, 2014a,b). Tree response to drought in interaction with K-fertilization starts to be well documented in organs such as leaves and roots (Cakmak, 2005; Anschütz *et al.*, 2014), but xylem has received much less attention. Most of the studies performed in this tissue focused on the

drought-induced structural modifications and their impact on water transport properties (Arend & Fromm, 2007; Zwieniecki & Secchi, 2015). Up to now, the changes occurring at the transcriptomic and metabolomic levels in xylem in response to drought and K-fertilization remain unstudied.

Wood formation is a highly regulated process mainly controlled at the transcriptional level and the expression of SCW-associated genes is tightly spatiotemporally regulated (Hertzberg *et al.*, 2001; Demura & Fukuda, 2007) through a complex hierarchical regulatory network (reviewed in Hussey *et al.*, 2013; Yang & Wang, 2016). Recent studies have highlighted the importance of a dynamic cross-talk between the regulation of SCW during development and in response to stresses, which is likely necessary to promote adaptation to environmental changes (Zinkgraf *et al.*, 2017). For instance, changes in thickness, composition and/or structure of SCW have been observed in response to several stresses such as nitrogen excess or depletion (Camargo *et al.*, 2014; Euring *et al.*, 2014), mechanic stress (Mellerowicz & Gorshkova, 2012) or cold temperature (Ployet *et al.*, 2018). Transcription factors (TFs) involved in the regulation of SCW formation as well as SCW biosynthesis genes were reported to be induced by environmental constraints such as high salinity or iron deprivation in *Arabidopsis* (Taylor-Teeples *et al.*, 2015) or cold stress in *Eucalyptus* (Ployet *et al.*, 2018). Some of these TFs were shown to be involved in stress tolerance (Ramírez *et al.*, 2011; Guo *et al.*, 2017).

To get a comprehensive view of a complex process such as the regulation of wood formation in response to environmental cues, system biology approaches seem the most adapted (Cramer *et al.*, 2011). Indeed, the integration of transcriptomic and metabolomic approaches has allowed gaining very valuable insights into the understanding of tension wood formation (Andersson-Gunnerås *et al.*, 2006) and in the lignin biosynthetic pathway (Vanholme *et al.*, 2012; Chen *et al.*, 2014) as well as in the primary wall transition to SCW (Li *et al.*, 2016b,a). Taylor-Teeples *et al.* (2015) constructed co-regulation networks inferred from protein-DNA interactions to refine the SCW regulatory network under abiotic stresses in *Arabidopsis* and highlighted new key regulators. In poplar, co-expression networks were used to identify cell-type specific TFs involved in the regulation of SCW biosynthesis in xylem (Shi *et al.*, 2017), and modules of genes involved in xylem formation under abiotic stresses (Cai *et al.*, 2014; Zinkgraf *et al.*, 2017; Wildhagen *et al.*, 2018). Mizrachi *et al.* (2017) have applied a network-based data integration method to reveal pathways underlying biomass and bioenergy-related traits using a segregating *Eucalyptus* hybrid population. Very recently, Wang *et al.*, (2018) developed a multi-omics integrative analysis of lignin

biosynthesis in poplar to quantify the effects of the expression of monolignol biosynthetic pathway genes on wood properties.

In order to get an integrated view of the regulation of wood formation in response to a combination of K and water regimes, we collected differentiating xylem from four-years *E. grandis* trees grown in four contrasting treatments. We performed both transcriptomic and metabolomic profiling to detect differentially expressed genes (DEGs) and differentially accumulated mass signatures (DAMs), respectively. We also evaluated trunk growth, xylem structure and saccharification yield as a proxy of changes in the SCW composition. We then constructed WGCNA (Weighted Gene Co-expression Network Analysis) and MixOmics-based co-regulation networks to correlate changes in transcriptome, metabolome and wood traits. This system biology approach enabled us to identify biological processes and meaningful subset of genes impacted by K-fertilization and/or water limitation. Among the latter, TFs highly connected to SCW biosynthetic genes and wood traits were highlighted as potentially involved in SCW regulation. We functionally characterized the most promising candidate and confirmed its ability to regulate SCW deposition in *E. grandis*.

2. Materials and Methods

2.1. Plant material and sampling

We took advantage of the experimental field trial set up in 2010 using a *E. grandis* commercial clone (Suzano Company, São Paulo) at the Itatinga Experimental Station of the University of São Paulo in Brazil (23°020S; 48°380W, for a detailed description see Battie-laclau *et al.* (2014a). Our study focused on four conditions combining potassium fertilization and water availability: (1) [+W-K] (No potassium (K) fertilization and no throughfall exclusion), (2) [-W-K] (No K-fertilization and 37% of throughfall excluded), (3) [+W+K] (0.45 mol K.m⁻² applied as KCl and no throughfall exclusion) and (4) [-W+K] (0.45 mol K.m⁻² applied as KCl and 37% throughfall exclusion). For each condition, phenotyping and xylem sampling were performed on four independent trees (**Fig. S1**).

Tree circumference (CBH) was measured at breast height (BH; 1,3m above ground) every 15 days. Trunk biomass was quantified after cutting down the trees as described in (Battie-Laclau *et al.*, 2016). An allometric equation allowing calculation of trunk biomass from CBH (González-García *et al.*, 2016) was applied to predict biomass production per day (kg of dry matter.d⁻¹.tree⁻¹) for each tree, over the 3 months preceding sampling. The daily average gross

primary productivity (GPP, $\text{gC}\cdot\text{m}^{-2}\cdot\text{day}^{-1}$) was estimated using the model established by Christina *et al.* (2015). The proportion of carbon allocated to trunk secondary growth ($\%\text{GPP}_{\text{stem}}$), was obtained for each tree by dividing the trunk biomass increment ($\text{kgDM}\cdot\text{d}^{-1}\cdot\text{tree}^{-1}$), by the simulated tree gross primary productivity ($\text{gC}\cdot\text{d}^{-1}\cdot\text{tree}^{-1}$).

Wood samplings were performed on four independent trees per condition (at BH) in May 2014, during a severe dry season (**Fig. S2**). Wood disks were collected for wood micro-density measurements and micro-core samples (length: 15mm; diameter: 2mm) were fixed and stored in 80% ethanol for histology analyses. Developing xylem (including cambium) was collected by scraping after removing the bark and immediately frozen in liquid nitrogen for transcriptomic and metabolomic analyses. Metabolome and wood properties were analysed on the four biological replicates for each condition and three replicates were used to perform transcriptomic analyses (**Fig. S3**).

2.2. RNA extraction and analyses of the transcriptome

RNA extraction and integrity controls were performed as previously described (Ployet *et al.*, 2018). Three sequencing libraries per treatment were generated and sequenced (Illumina, 150 bp paired-end reads) by the Genotoul GeT platform (<https://get.genotoul.fr/en/>; France) using the HiSeq3000 (Illumina). An average of 46 million reads per library was generated, >90% were mapped to *E. grandis* reference genome (v1.1, <https://phytozome.jgi.doe.gov/>) using TopHat2 (Kim *et al.*, 2013). Sequencing data were registered at NCBI SRA databases (PRJNA514408). For a subset of selected genes, RNAseq expression levels were confirmed by RT-qPCR (**Fig. S4, Table S1**) as described in (Ployet *et al.*, 2018).

2.3. Metabolites extraction and biochemical analyses

Soluble metabolites were extracted from 4 independent biological replicates and analyzed according to the methods described by De Vos *et al.*, 2007 and (Hoffmann *et al.*, 2017) for GC-MS and LC-MS, respectively including minor changes detailed in **Method S2**. Biochemical analyses of SCWs were done in triplicate from extractive-free xylem residues (EXR) obtained as previously described in Ployet *et al.* (2018) and detailed in **Method S1**. Saccharification was estimated with or without alkali pre-treatment, mainly as described in Van Acker *et al.* (2016). Reducing sugar concentration was assessed with dinitrosalicylic acid

(DNS) reagent using a 10µl aliquot of the supernatant after 6h, 24h and 48h of reaction. Enzyme activity was assessed at 0.25 FPU/ml in our conditions.

2.4. Vector construction and plant transformation

The coding region (1050bp) of *EgMYB137* (*Eucgr.K02806*), and a fragment of 2kb upstream of the start codon (promoter) were amplified from *E. grandis* xylem cDNA and genomic DNA, respectively using specific primers (**Table S1**). The DNA fragments were then cloned into Gateway-adapted binary vectors pGWAY-0 and pGWAY-1, for overexpression and promoter activity analyses respectively and transformed into *Eucalyptus* hairy roots as described in Plasencia *et al.* (2016). *Eucalyptus* composite plants harboring transgenic hairy roots were grown in OIL DRI substrate US-Special Substrate (Type III/R; Damolin, Fur, Denmark) in 200-mL pots for a period of 5 months (16 h photoperiod, 25/22°C). Fluorescent roots expressing DsRed were collected on 7 to 9 independent lines for further analyses. Histochemical GUS assays were performed as described in Plasencia *et al.* (2016).

2.5. Microscopy and histochemistry

Wood density was measured as described in Dobner *et al.* (2018). The average density (g.cm⁻³) was measured by X-ray every 40 µm along the first 4 mm of differentiating xylem zone using a QTRS-01X Tree Ring Analyzer according to manufacturer procedure (Quintek Measurement Systems, Knoxville, TN. 1999). For xylem structure analysis, transverse sections were made from micro-cores samples (3 biological replicates per condition) and transgenic roots (six *p35S:EgMYB137* lines and four controls), and embedded in LR White resin (London Resin Company Ltd). Semi-automatic image analyses of semi-thin sections (1µm) were performed as previously described (Ployet *et al.*, 2018) to estimate SCW thickness (**Method S1**). Average vessel diameter was measured by image analyses on >400 vessels (diameter cut-off >35 µm) using Image J software (v1.5).

2.6. Statistical analyses and data integration

For transcriptomic analyses, we combined CuffDiff v2.2.1 (Trapnell *et al.*, 2012) and DEseq2 R package v1.10 (Love *et al.*, 2014) to detect, a total of 5,573 differentially expressed genes (fold change ≥ 2 , adjusted *P-value* (FDR) < 0.01 , **Table S1**). For metabolomic analyses, 2,250 mass signatures were obtained by LC-MS (850) and GC-MS (1400). Mass signatures detected in less than 2 technical repetitions and 2 conditions were discarded. We identified 516 differentially accumulated mass signatures (DAMs), 231 and 285 for LC-MS and GC-MS respectively (fold change ≥ 2 , FDR < 0.01 , **Table S2**). Missing values were substituted by random forest imputation (Gromski *et al.*, 2014), using missForest R package (Stekhoven & Buhlmann, 2012). In total 6,089 DEGs and DAMs were used to perform datamining. Discrimination of the different treatments and biological replicates was done using Partial Least Square - Discriminant Analysis (PLS-DA), from R package mixOmics (Lê Cao *et al.*, 2016).

We used BiNGO package (Cytoscape© software, Maere *et al.*, 2005) and g:Profiler (Reimand *et al.*, 2016) to perform gene ontology enrichment based on *Arabidopsis thaliana* GO classification on the first blast hit of *Eucalyptus* DEGs in *Arabidopsis* genome (Phytozome V12). Two networks of GO enrichment were obtained for genes regulated by either water availability (+W treatments *versus* -W treatments) or K supply (+K treatments *versus* -K treatments). They were merged and manually curated to remove redundant GO terms (**Fig. 2**).

Network analyses based on Pearson pairwise correlations, calculated from three values per condition, were performed as described previously (Ployet *et al.*, 2018). We used WGCNA method (Langfelder & Horvath, 2008) to detect modules (softPower=10, deepSplit=3 and minModuleSize=100) and compute correlations between average module profiles and phenotypic variables. Correlations between standardized profiles of DAMs and DEGs of modules M1 to 6, were further investigated using mixDIABLO (Data Integration Analysis for Biomarker discovery using a Latent component method for Omics studies, Singh *et al.*, 2016). In the sparse Partial Least Square Discriminant Analysis (sPLS-DA), a full design was chosen in which all datasets are connected, all variables were kept and number of components set to 3. Correlation values (**Table S3**) were used to graphically represent networks using Cytoscape© software. For WGCNA, significant Pearson correlations were used (FDR $< 5.10e-5$) to select 4305 nodes. For MixOmics, a correlation threshold of 0.8

within mixDIABLO similarity matrix was chosen to optimize modularity and allow comparison with WGCNA network (**Fig. S5**).

3. Results

3.1. Remodelling of the xylem transcriptome and metabolome in response to K-supply and water availability

The analyses of the transcriptome and the metabolome of differentiating xylem tissues collected from field-grown *E. grandis* trees submitted to four different treatments combining rainfall water availability and K fertilization (**Fig. 1a,b**), revealed a total of 5,573 differentially expressed genes (DEGs) and 516 differentially accumulated mass signatures (DAMs, **Fig. 1c,d, Table S1 and S2**), respectively. The four treatments were clearly separated by the first three principal components (PC) of the Partial Least Squares - Discriminant Analysis (PLS-DA), explaining 82% and 76% of the total variance of the DEG expression profiles and of the abundance profiles of DAMs, respectively (**Fig. 1c,d, Fig. S3**). The first component (PC1) explained the highest percentage of variance (61% for DEGs and 39% for DAMs) clearly separating K-fertilized [+K] from non-fertilized [-K] samples. Indeed, most of the DEGs (>60%, **Fig. 1c**) and a large proportion of the DAMs (42%, **Fig. 1d**) were exclusively regulated by K-fertilization. In sharp contrast, 4% of the DEGs and 12% of the DAMs were regulated by water availability only. Interestingly, a substantial percentage of the DAMs (45%) and of the DEGs (34,7%) was regulated by both water and K. The vast majority of the DEGs (90%) and DAMs (79%) regulated by water were also regulated by K whereas only 36% of the DEGs and 52% of the DAMs regulated by K were also regulated by water.

Using a Gene Ontology (GO) enrichment approach, we found that 159 biological processes (**Fig. 2, Table S1**) were significantly enriched among the DEGs. We made a hierarchical classification of these GO categories from the most general to the most specialized level (level 9, 45 GOs) and represented by green, blue and grey dots, the categories enriched in K-regulated, W-regulated and [K and/or W]-regulated DEGs, respectively. Considering level 9-GO categories, 23 were enriched in K-regulated DEGs, mainly related to development, primary metabolism, cell wall formation, regulatory processes, transport and abiotic stresses. The fifteen GOs enriched in K and/or W-regulated DEGs, were related to secondary metabolism, biotic and abiotic stress responses and

biological regulation. Only 7 GOs were enriched in W-regulated DEGs and included abiotic stresses responses and transport.

3.2. Integration of transcriptomic and metabolomic data through correlations network analyses

In order to get insights into the regulation of xylem transcriptome and metabolome, we analysed the correlations between 6,089 variables representing 5,573 DEGs and 516 DAMs (**Table S3**). We performed a correlations network analysis based on Pearson pairwise correlations to detect gene-gene or gene-metabolite profiles similarities. We selected the most robust correlations (FDR adjusted p value $< 5.10 \times 10^{-5}$) to build a network in which 4,305 nodes (representing either DEGs or DAMs) were connected by 170,629 edges whose lengths were proportional to the absolute values of the corresponding correlations (**Fig. 3**). We obtained a dense, strongly correlated core network linked to six small subnetworks (**Fig. 3**). Sixty percent of the 155 DAMs were spread across the network and correlated to DEGs but the remaining 40% were clustered in a specific subnetwork poorly connected with DEGs (i.e. only 6 DAMs were connected to DEGs).

Using the WGCNA method, we detected 12 modules containing highly correlated variables and therefore potentially involved in the same biological process (**Fig. 3**). For each module, we performed a GO enrichment analysis (**Table S1**) and represented by heatmaps DEGs' profiles in the four treatments (**Fig. 3**). The expression profiles of the genes in all modules, except module 12, were more dependent on K-fertilization than on water status (**Fig. S6**).

The modules M1 to M5 located in the core of the network, were enriched in cell wall-related genes, especially in genes involved in the synthesis and in the regulation of the three main SCW polymers (cellulose, xylan, lignin) (**Fig. 3, Table S4**). Most of these genes (80%) were down-regulated in response to K-fertilization while the remaining 20% mostly involved in cell primary metabolism, were up-regulated and thus negatively correlated with the first ones. (**Table S2**). This included *EgrNAC12*, a putative ortholog of the drought inducible *ANAC002* in *Arabidopsis* (**Table S4**). Among the K-down-regulated genes, 109 TFs were identified including regulators acting in the early phase of xylem differentiation like *AtWRKY12*, *AtWRKY13*, *AtIFL1/REV*, *ATHB8* and *ATHB15* (**Table S4**). Twenty-three TFs were orthologs of the regulators belonging to SCW hierarchical transcriptional network in *Arabidopsis* (**Table S4**) such as *EgrNAC61* and *EgrNAC26*, orthologs of first level master

switches *AtSND1* and *AtVND6*, respectively. The second level positive (*EgMYB2*) and negative (*EgMYB1*) master switches functionally characterized in *Eucalyptus* were also present (Goicoechea *et al.*, 2005; Legay *et al.*, 2007). Fifty-two DAMs (33%) were correlated with the M1 to M5 modules with M2 presenting the highest number of connected DAMs.

Nested in the core of the network, the M6 module was highly connected with M1 to M5 and significantly enriched with genes involved in cytoskeleton remodeling. No DAMs was linked to M6. Noteworthy, the Rac-like small GTPase *EgROP1*, **Table S4**, previously shown to be involved in the control of cell morphology and SCW formation in *Eucalyptus* xylem (Foucart *et al.*, 2009), was among the most connected genes. M6 also contained orthologs of genes involved in vesicle trafficking of CW polymers and CW modifying enzymes, through interaction with microtubules like *AtAAA1*, *AtRABA5a*, *AtRABA4a* and *AtROPGAP3* (**Table S4**).

The modules M10 and M11 were enriched in genes related to cell activity (RNA and protein metabolisms) and to abiotic stresses responses such as genes encoding heat shock proteins, ROS detoxification enzymes, secondary metabolism enzymes, stachyose and polyamine biosynthesis enzymes (**Table S4**). These modules contained orthologs of most of the key components of the ABA signaling pathway (**Table S4**), including receptors (*AtRCAR1/AtPYL9*, *AtRCAR3/AtPYL8*), receptor-associated kinase (*AtSnRK2.6/AtOST1*) and kinase's direct substrate (*AtAREB3*). ABA-inducible TFs, like *ATHB7*, *ANAC081* and *ANAC102* (**Table S4**) were also present, as well as *AtRAE1* (ABA signaling) and *AtXERICO* (ABA metabolism). All these genes were strongly up-regulated in response to K-fertilization and especially when water was available [+W+K]. M10-M11 DEGs were connected with 19 DAMs.

M7 and M12 were enriched in genes strongly regulated by water in addition to be regulated by K (**Fig. S6**). Most of the genes of M7, related to "DNA replication and cell cycle", were down-regulated by water exclusion in K-deficient trees, but up-regulated by water exclusion in K-fertilized trees. Among these DEGs, 29 out of 126 belong to cell division machinery, chromosome segregation and cytokinesis (**Table S4**) including cyclin dependent kinases, like *Eucgr.A00867*, a putative ortholog of *AtCDKB2;2* required for meristem integrity in *Arabidopsis*. *EgrAP2-11*, the only detected TF in M7 is a putative ortholog of *AtANT*, associated to cell division regulation in *Arabidopsis* shoot meristem (**Table S4**). M12 was enriched in genes related to transport of molecules that were up-regulated in [-W-K] treatment. Nine encode proteins similar to transporters essential for xylem development or sap transport in *Arabidopsis* such as possible orthologs of

AtABCG11 and *AtABCB15* required for vascular development, and a close ortholog of *AtWAT1*, a tonoplast-localized transporter involved in SCW biosynthesis of xylem fibers in *Arabidopsis* (Table S4). Only one DAM was connected with M12 DEGs.

The M8 and M9 modules both contained genes up-regulated by water exclusion in K-fertilized trees (Fig. S6). M8 enclosed genes related to cambial activity, like several components of the *CLAVATA* peptide signaling pathways, as well as genes close to *AtMOL1* receptor and its ligand *AtCLE44/TDIF* (Table S4). Among the putative TFs detected in M8, we found orthologs of *AtDof5.6* and *AtARF4* which are involved in the formation of interfascicular cambium and vascular patterning in *Arabidopsis* roots, and in promoting cambium activity respectively (Table S4). Orthologs of genes related to K-homeostasis (*AtSKOR* and *AtZIFL2*) and to calcium sensing and transport (*AtSOS3*, *AtCAX1*, *AtCAX3* and *AtCAX7*) were also found in M8. The M9 module was enriched in genes related to phloem development (Table S4), like putative orthologs of *AtSEOR1* required for phloem filament formation and orthologs of *AtAPL* required for phloem identity in *Arabidopsis*. Sixteen DAMs were associated to M8-M9.

3.3. Correlations between identified DAMs and network modules

In an attempt to optimize the integration of the metabolomic and transcriptomic datasets, we decided to use the mixDIABLO method of MixOmics R package, a method designed for testing correlations between heterogeneous “Omics” datasets. As shown in Fig. 4a, where the correlations between DAMs and modules are represented, the number of highly connected DAMs (282) was substantially increased as compared to the first method where only 93 were correlated with DEGs (Fig. 3). None of the DAMs was connected to the M7 and M12 modules in agreement with the first correlation analysis. The vast majority of the highly connected DAMs (213, 76% of the DAMs) were associated with the modules M1 to M6 related to cell wall formation and cytoskeleton. Most of these DAMs accumulated in [+K] conditions and were negatively correlated to expression profiles of SCW-related genes. Among the most connected DAMs (red diamonds, Fig. 4a), 37 were selected for LC-MS-MS analyses and 14 provided robust identification. They belong mostly to the flavonoids, coumarins and terpenes categories, but also to lipid and amino acids derivatives (Fig. 4b). Twelve were clearly accumulated in [+K] conditions and two in [-W] conditions.

3.4. Correlations between wood properties and network modules

The quantification of phenotypic traits related to wood formation in the four treatments (**Fig. 5**) revealed that the saccharification yield, vessel density and vessel diameter were almost exclusively regulated by K-fertilization whereas stem biomass increments and wood density were affected by both water exclusion and K-fertilization. Saccharification yield and vessel density significantly decreased (-14% and -16% respectively) in K-deficient trees relative to K-fertilized trees. In contrast, vessel diameter increased significantly in K-fertilized trees and slightly more when water was excluded (+15%, **Fig. 5**). Stem biomass increments were the highest in K-fertilized trees but were significantly reduced by water exclusion. Wood density tended to increase in response to water exclusion, but only significantly for K-fertilized trees (**Fig. 5**). The lowest carbon allocation for trunk growth (GPPstem) was found in [-W-K] treatment whereas unexpectedly the highest value was found in the [-W+K] treatment.

We then used the WGCNA method to compute the correlations between the module profiles (mean profiles of all the variables contained in a module) of M1 to M12 and the phenotypic traits. In the network represented **Fig. 5**, the phenotypic traits were correlated with the 12 modules profiles as well as with 2,184 variables contained in these modules (2,148 DEGs and 36 DAMs). The core-network modules M1 to M6 were positively correlated with vessel density and saccharification yield (**Fig. 5**). In contrast, these modules, except M2, were negatively correlated to vessel diameter (**Fig. 5**). The correlations obtained between traits and module profiles reflected well the correlations between traits and variables (**Fig. S7, Table S3**). Indeed, most of the 1,554 variables in modules M1 to M6 were positively correlated (1,187 variables) with saccharification and vessel density, whereas 720 variables were negatively correlated with vessel diameter. Stem biomass increments were positively correlated with modules M10 and M11 but negatively with modules M4 and M5. Wood density was positively correlated with modules M8 and M9 that were negatively correlated to saccharification yield. Module M8 was also positively correlated to vessel diameter. GPPstem was positively correlated with module M7 and negatively with M12.

3.5. Identification of TFs related to wood formation in response to water exclusion and K-fertilization

With the aim of identifying new transcription factors (TFs) involved in wood formation and regulated by K-fertilization and/or W status, we extracted from modules M1 to M6 (**Fig. 3,4**), a subnetwork containing 113 genes known to be involved in SCW biosynthesis (**Fig. 6**). All the genes present in this subnetwork were tightly co-expressed and strongly down-regulated by K-fertilization. Their expression profiles were positively correlated to saccharification yield, and vessel density but negatively correlated to vessel diameter. Among the SCW-associated DEGs, 65 were correlated to wood phenotypic traits and to identified DAMs (**Fig. 6, Table S3**). Sixteen of them were orthologs of TFs known to regulate SCW biosynthesis (**Table S4**) while 32 TFs were not yet functionally characterized in *Arabidopsis* nor *Populus*. We examined their connectivity in networks, their expression profiles in EucGenIE (<https://eucgenie.org/>) and their presence in previous data integration studies in *Arabidopsis*, *Populus* and *Eucalyptus* (**Fig. 6, Table S5**). *EgMYB137* obtained the best score in the ranking of the 32 TFs. It was correlated to 22 SCW biosynthesis genes and 5 SCW-TFs which were the closest orthologs of *AtSND1*, *AtNST1*, *AtMYB46*, *AtMYB83* and *AtC3H14* (**Table S4**). Noteworthy, we found that this *EgMYB137*'s subnetwork was conserved in both *P. trichocarpa* and *A. thaliana* (**Fig. S8**).

3.6. *EgMYB137* is a regulator of xylem formation in *Eucalyptus*

In order to functionally characterize this promising new candidate, we investigated its spatial expression using *E. grandis* transgenic hairy roots transformed with a promoter-GUS fusion and overexpressed its coding sequence under the control of the CamV35S promoter. Histochemical analyses revealed that *EgMYB137* promoter drives GUS activity in the vascular cylinder of young roots (**Fig. 7a**) and in parenchyma cells surrounding developing vessels close to the cambial zone in older roots (**Fig. 7b-d**). Cross sections of transgenic roots ongoing secondary growth revealed an enhanced deposition of SCW in xylem (**Fig. 7e,f**). The SCW of fibers of the *p35S:EgMYB137* lines were significantly thicker (+12%) as compared to control lines. In contrast, the SCW of vessels were significantly thinner in *p35S:EgMYB137* (-4%), as compared to control lines (**Fig. 7g**). The vessel density was significantly reduced (-35%) in *p35S:EgMYB137* as compared to control lines (**Fig. 7h**) but no significant change in vessel nor fibre lumen diameter was observed (**data not shown**). We

Accepted Article
further investigated the consequences of *EgMYB137* overexpression on the saccharification yield (**Table 1**). With or without pre-treatment, the saccharification yield was reduced of approximately 16% in *35S::EgMYB137* lines as compared to control lines.

4. Discussion

4.1. K-fertilization and water availability trigger interconnected regulations in xylem

We developed a system biology approach that enabled us to get a comprehensive view of the regulations involved in wood formation of field-grown *E. grandis* trees submitted to four treatments combining K-fertilization and rainfall water availability. In our conditions, K-fertilization was responsible for (i) the highest proportion of DEGs and DAMs, (ii) the highest proportion of variance explained by PLS-DA and (iii) the highest proportion of enriched GO categories. Most of these GO categories were related to development, primary metabolism and cell wall biosynthesis. Most of the genes of the co-expression network (modules M1 to M12), were strongly regulated by K-fertilization with no or minor impact of water exclusion. These findings, demonstrating the prevailing impact of K on the remodeling of the transcriptome and the metabolome, are in line with our previous physiological studies on three-year old trees showing that regardless water supply, K-fertilization increased dramatically gross primary productivity and above-ground biomass production (Battie-Laclau *et al.*, 2014a,b ; Christina *et al.*, 2015). Similarly, we observed an increase of stem biomass increments in K-fertilized trees.

In response to water exclusion, enriched GO categories were mainly related to stress response and molecule transport but a high proportion of the stress-related genes were also differentially regulated by K-supply. The separation between [-W] from [+W] treatments by PLS-DA was highly dependent on K-fertilization suggesting that trees' response to water shortage is highly dependent on K-availability. On the other hand, genes in module M10 and M11, involved in abiotic stress response and containing numerous genes of ABA signaling pathway, were highly up-regulated in either [-W+K] or [+W+K] treatments suggesting that K-fertilized trees were stressed independently of water availability. This finding is consistent with previous physiological studies showing that at end of dry season, K-fertilized trees reached a higher level of water stress than K-deficient trees (Battie-Laclau *et al.*, 2014a,b; 2016). This drought-induced effect of K-fertilization was linked to the enhancement of tree growth rate causing a faster decrease in soil water stocks during dry periods (Christina *et al.*,

2018). This was particularly true in our study because of the exceptionally low amount of rainfall during the months preceding sampling (**Fig. S2**). Trees grown in [-W+K] underwent continuous drought episodes and developed adaptive traits to survive (Battie-Laclau *et al.*, 2014a,b; 2016). In comparison, trees grown in [+W+K] were less acclimated to severe drought event. In agreement with this hypothesis, [-W+K] trees exhibited a highest GPP stem than [+W+K] and the highest expression level of stress responsive genes (modules M10 and M11), such as the drought responsive TF *EgDREB2.5* (**Fig. S4**), was observed in [+W+K] treatment relative to [-W+K]. DEGs involved in secondary metabolism (M9 module) and most of the (LC-MS) DAMs were also strongly induced in K-fertilized trees. Among the latter, the 14 identified could be related to drought stress response as signaling lipids (Hou *et al.*, 2016) or anti-oxidant compounds like flavonoids, terpenoids and coumarins (Karabourniotis *et al.*, 2014).

4.2. SCW formation in the heart of xylem response to K-fertilization and water supply

The SCW modules (M1 to M6) constitute the core of the network and the vast majority of the SCW-associated genes were drastically down-regulated in response to K-fertilization suggesting a reduction or a delayed SCW deposition in developing xylem cells. These six modules were strongly correlated with saccharification yield which reflects the accessibility of cell wall polysaccharides to enzymatic degradation, and is a crucial parameter for second-generation biofuel production (Van Acker *et al.*, 2014). A subset of genes in M1 to M6, associated to primary metabolism, were negatively correlated with the SCW-associated genes and up-regulated in K-fertilized trees. Among them, we found *EgrNAC12*, a putative ortholog of *ANAC002*, an ABA-inducible key TF strongly up-regulated in response to cellular carbon depletion in *Arabidopsis* and responsive to stress including drought (Garapati *et al.*, 2015). Considering the fact that K-fertilization triggers drought stress signaling in our conditions, one possible hypothesis could be that K-fertilized trees develop strategies to mitigate drought stress like stomatal closure to reduce transpiration, resulting in a reduction of carbon fixation by photosynthesis. Prolonged episodes of drought are known to lead to a lower carbon uptake and consequently to carbon starvation for all tree organs (Mitchell *et al.*, 2014). K-fertilized trees could therefore modify carbon allocation at the detriment of SCW biosynthesis as suggested by the repression of genes related to nucleotide-sugars (like UDP-Galactose transporters), often included within SCW modules (Li *et al.*, 2016b). Similarly, the accumulation of 80% of DAMs, negatively correlated with SCW-

DEGs, could be at least partially a consequence of the repression of a phenylpropanoid pathway 's branch (Vanholme *et al.*, 2012).

Another hypothesis not exclusive of the first one is that like in poplar, SCW deposition could be delayed in K-fertilized trees as a result of a stimulation of cambial activity (Langer *et al.*, 2002). In support of this hypothesis, we detected two groups of modules (M8-9 and M10-11) associated to cambial activity, cell activity and metabolism that were induced in response to K-fertilization. The expression profiles of these genes which were also positively correlated with trunk biomass increments and wood density, pointed to a positive effect of K-fertilization on cambial activity and cell metabolism. This agrees with the essential role of K in cambial activity maintenance (Fromm, 2010). According to Langer *et al.* (2002), the osmotic role of K is also essential for vessel expansion. Modules M1 to M6 were correlated negatively with vessel diameters and positively with vessel density that increased, and decreased respectively in response to K-fertilization. Besides enhancing transport efficiency, wider vessels can increase the vulnerability of xylem to cavitation, making trees more sensitive to drought episodes although other parameters like vessel SCW composition and structure also influence xylem cavitation (Hacke *et al.*, 2001).

Up to date, most of the systems biology studies performed on woody tissues, focused on SCW, only few uncovered genes involved in cambial activity (Zinkgraf *et al.*, 2017; Ployet *et al.*, 2018). In the present study, the fine sampling of immature cells between bark and differentiating xylem, allowed the identification of 18 TFs as promising candidates for the control of cambial activity in response to K-fertilization and water exclusion.

4.3. Integrative approach linked meaningful genes to complex traits

Within the core SCW modules (M1 to M6), 56 TFs correlated to SCW genes and wood traits. These known and potential SCW-related TFs, down-regulated in response to K fertilization and to a lesser extent by water shortage, likely play a role in the adaptation of trees to these environmental cues through modification of SCW properties and/or xylem anatomy. For instance, the strong down-regulation of the SCW positive master switch such as *EgMYB2* suggests that SCW deposition in fibers cells is dramatically reduced in K-fertilized trees. Similar profiles were observed for a suite of TFs (*EgMYB31*, *EgMYB60*, *EgMYB80*, *EgMYB122*, *Eucgr.F02796*, *Eucgr.D01219* and *Eucgr.D01935*) which are the orthologs of TFs regulating SCW deposition in *Arabidopsis* *AtMYB83*, *AtMYB103*, *AtMYB69*, *AtMYB43*, *AtC3H14*, *AtWRKY12* and *AtKNAT7* respectively. TFs described in the literature as positive and negative regulators of SCW deposition (Hussey *et al.*, 2013) were both poorly expressed

in K-treatments suggesting that xylem differentiation is slowed down at the benefit of cambial cell proliferation. In fully elongated immature xylem cells of *Arabidopsis*, SCW deposition is activated by either *AtSND1* and *AtNST1/2* in fibres or *AtVND6* and *AtVND7* in vessels (Zhong *et al.*, 2006; Mitsuda *et al.*, 2007; Yamaguchi *et al.*, 2010). SCW modules contain *EgNAC61* and *EgNAC49*, the closest orthologs of *AtSND1* and *AtNST1/2*, but no putative orthologs of the VND TFs (Vascular NAC Domain). The absence of significant down-regulation of VND master switches suggests that the deposition of SCW in vessels is moderately impacted by fertilization, possibly to preserve the integrity of vessels SCW, essential for water transport. Similarly, we observed an opposite pattern of SCW deposition in fibers and vessels of 35S::*MYB137* transgenic roots (**Fig. 7**). *EgMYB137* appeared as the best candidate from a list of 32 TFs of unknown function, tightly correlated with a high number of known SCW biosynthesis genes as well as with wood properties (saccharification yield and vessel properties). To our knowledge, these TFs highly expressed in xylem, or their close orthologs, have never been characterized although they have been detected in other system biology studies (**Table S5**). Some of them were co-expressed with SCW related genes or direct targets of SCW regulators in *Arabidopsis* and *Eucalyptus* (**Table S5**). In poplar, putative orthologs for 22 of them were clustered in wood related modules together with SCW genes (**Table S5**). *EgMYB137*, a member of the large R2R3MYB family (Soler *et al.*, 2015), showed the highest-ranking score among all candidates (**Table S5**).

4.4. The highly connected xylem specific TF *EgMYB137* can regulate SCW deposition

The functional characterization of *EgMYB137* strongly support that this TF regulates SCW formation as inferred from the network where it was correlated with saccharification yield, vessel density, vessel diameter: i) *EgMYB137* promoter is specifically active in developing vessels and surrounding axial parenchyma, ii) in *EgMYB137* overexpressing lines, cell wall thickness increases whereas vessel density and saccharification markedly decrease. Based on the positive correlations between *EgMYB137* expression profiles and both saccharification and vessel density, it was unexpected to observe a decrease of both in the transgenic overexpressing hairy roots. This apparent discrepancy might reflect the complex mode of regulation of some TFs that can have a dual function depending on their expression level (dose-dependent effect) and the abundance of additional regulator proteins. This was clearly illustrated for *SND2* a well-known SCW TF, whose overexpression could increase SW deposition within a limited range of overexpression levels (Hussey *et al.*, 2011). Above a

certain level, *AtSND2* overexpression, had a negative effect on interfascicular fibers SCW deposition in *Arabidopsis* (Hussey *et al.*, 2011). More investigations are required to define the mode of action of *EgMYB137* but our data clearly demonstrated that it has an important role in the regulation of wood formation. These result also strongly support SCW- regulatory roles for the 31 other TFs that deserve to be functionally characterized and further highlight the powerfulness of the network approach developed here.

In conclusion, our network-based approach revealed that co-regulated genes and metabolites modules related to wood formation are at the heart of a complex trade-off between secondary growth and stress response. Nested in these modules, new uncharacterized TFs were pointed out, potentially involved in SCW remodeling in stress conditions, leading to adaptive wood traits. We demonstrated that the most promising of them, the TF *EgMYB137*, was involved in the regulation of xylem structure and composition. All together, this study represents an original attempt to correlate molecular regulations and complex wood traits in xylem.

5. References

- Andersson-Gunnerås S, Mellerowicz EJ, Love J, Segerman B, Ohmiya Y, Coutinho PM, Nilsson P, Henrissat B, Moritz T, Sundberg B. 2006. Biosynthesis of cellulose-enriched tension wood in *Populus*: global analysis of transcripts and metabolites identifies biochemical and developmental regulators in secondary wall biosynthesis. *The Plant journal : for cell and molecular biology* **45**: 144–165.
- Anschütz U, Becker D, Shabala S. 2014. Going beyond nutrition: Regulation of potassium homeostasis as a common denominator of plant adaptive responses to environment. *Journal of Plant Physiology* **171**: 670–687.
- Arend M, Fromm J. 2007. Seasonal change in the drought response of wood cell development in poplar. *Tree physiology* **27**: 985–92.
- Arend M, Monshausen G, Wind C, Weisenseel MH, Fromm J. 2004. Effect of potassium deficiency on the plasma membrane H⁺-ATPase of the wood ray parenchyma in poplar. *Plant, Cell and Environment* **27**: 1288–1296.
- Arend M, Weisenseel MH, Brummer M, Osswald W, Fromm JH. 2002. Seasonal changes of plasma membrane H⁺-ATPase and endogenous ion current during cambial growth in poplar plants. *Plant physiology* **129**: 1651–1663.
- Battie-Laclau P, Delgado-Rojas JS, Christina M, Nouvellon Y, Bouillet J-P, Piccolo M de C, Moreira MZ, Gonçalves JL de M, Rouspard O, Laclau J-P. 2016. Potassium fertilization increases water-use efficiency for stem biomass production without affecting intrinsic water-use efficiency in *Eucalyptus grandis* plantations. *Forest Ecology and Management* **364**: 77–89.
- Battie-laclau P, Laclau J-P, Beri C, Mietton L, Muniz MRA, Arenque BC, De Cassia Piccolo M, Jordan-Meille L, Bouillet J-P, Nouvellon Y. 2014. Photosynthetic and anatomical responses of *Eucalyptus grandis* leaves to potassium and sodium supply in a field experiment. *Plant, Cell & Environment* **37**: 70–81.
- Battie-Laclau P, Laclau J-P, Domec J-C, Christina M, Bouillet J-P, de Cassia Piccolo M, de Moraes Gonçalves JL, e Moreira RM, Krusche AV, Bouvet J-M, *et al.* 2014. Effects of potassium and sodium supply on drought-adaptive mechanisms in *Eucalyptus grandis* plantations. *New Phytologist* **203**: 401–413.
- Bonan GB. 2008. Forests and Climate Change: Forcings, Feedbacks, and the Climate Benefits of Forests. *Science* **320**: 1444–1449.
- Cai B, Li C-H, Huang J, Reuber L, Jiang C. 2014. Systematic Identification of Cell-Wall Related Genes in *Populus* Based on Analysis of Functional Modules in Co-Expression Network (K Mills, Ed.). *PLoS ONE* **9**:

Cakmak I. 2005. The role of potassium in alleviating detrimental effects of abiotic stresses in plants. *Journal of Plant Nutrition and Soil Science* **168**: 521–530.

Camargo ELO, Nascimento LC, Soler M, Salazar MM, Lepikson-Neto J, Marques WL, Alves A, Teixeira PJPL, Mieczkowski P, Carazzolle MF, et al. 2014. Contrasting nitrogen fertilization treatments impact xylem gene expression and secondary cell wall lignification in *Eucalyptus*. *BMC plant biology* **14**: 256.

Chen H-C, Song J, Wang JP, Lin Y-C, Ducoste J, Shuford CM, Liu J, Li Q, Shi R, Nepomuceno A, et al. 2014. Systems Biology of Lignin Biosynthesis in *Populus trichocarpa*: Heteromeric 4-Coumaric Acid:Coenzyme A Ligase Protein Complex Formation, Regulation, and Numerical Modeling. *The Plant cell* **26**: 876–893.

Christina M, Le Maire G, Battie-Laclau P, Nouvellon Y, Bouillet J-P, Jourdan C, de Moraes Gonçalves JL, Laclau J-P. 2015. Measured and modeled interactive effects of potassium deficiency and water deficit on gross primary productivity and light-use efficiency in *Eucalyptus grandis* plantations. *Global Change Biology* **21**: 2022–2039.

Christina M, le Maire G, Nouvellon Y, Vezy R, Bordon B, Battie-Laclau P, Gonçalves JLM, Delgado-Rojas JS, Bouillet J-P, Laclau J-P. 2018. Simulating the effects of different potassium and water supply regimes on soil water content and water table depth over a rotation of a tropical *Eucalyptus grandis* plantation. *Forest Ecology and Management* **418**: 4–14.

Cramer GR, Urano K, Delrot S, Pezzotti M, Shinozaki K. 2011. Effects of abiotic stress on plants: a systems biology perspective. *BMC plant biology* **11**: 163.

Demura T, Fukuda H. 2007. Transcriptional regulation in wood formation. *Trends in Plant Science* **12**: 64–70.

Dobner M, Huss J, Tomazello Filho M. 2018. Wood density of loblolly pine trees as affected by crown thinnings and harvest age in southern Brazil. *Wood Science and Technology* **52**: 465–485.

Dunisch O, Bauch J, Muller M, Greis O. 1998. Subcellular quantitative determination of K and Ca in phloem, cambium, and xylem cells of spruce (*Picea abies* [L.] Karst.) during earlywood and latewood formation. *Holzforschung* **52**: 582–588.

Epron D, Laclau J-P, Almeida JCR, Gonçalves JLM, Ponton S, Sette CR, Delgado-Rojas JS, Bouillet J-P, Nouvellon Y. 2012. Do changes in carbon allocation account for the growth response to potassium and sodium applications in tropical *Eucalyptus* plantations? *Tree Physiology* **32**: 667–679.

Euring D, Bai H, Janz D, Polle A. 2014. Nitrogen-driven stem elongation in poplar is linked with wood modification and gene clusters for stress, photosynthesis and cell wall formation. *BMC plant biology* **14**: 391.

Foucart C, Jauneau A, Gion J-M, Amelot N, Martinez Y, Panegos P, Grima-Pettenati J, Sivadon P. 2009. Overexpression of EgROP1, a *Eucalyptus* vascular-expressed Rac-like small GTPase, affects secondary xylem formation in *Arabidopsis thaliana*. *New Phytologist* **183**: 1014–1029.

Fromm J. 2010a. Wood formation of trees in relation to potassium and calcium nutrition. *Tree physiology* **30**: 1140–1147.

Fromm J. 2010b. Wood formation of trees in relation to potassium and calcium nutrition. *Tree Physiology* **30**: 1140–1147.

Garapati P, Feil R, Lunn JE, Van Dijck P, Balazadeh S, Mueller-Roeber B. 2015. Transcription Factor *Arabidopsis* Activating Factor1 Integrates Carbon Starvation Responses with Trehalose Metabolism. *Plant Physiology* **169**: 379–390.

Goicoechea M, Lacombe E, Legay S, Mihaljevic S, Rech P, Jauneau A, Lapierre C, Pollet B, Verhaegen D, Chaubet-Gigot N, et al. 2005. EgMYB2, a new transcriptional activator from *Eucalyptus* xylem, regulates secondary cell wall formation and lignin biosynthesis. *Plant Journal* **43**: 553–567.

Gonçalves JLM, Barros NF, Nambiar EKS, R.F. N. 1997. Soil and stand management for short-rotation plantations. In: Nambiar E.K.S. BAG, ed. Management of Soil, Nutrients and Water in Tropical Plantation Forests. Canberra, Australia: Australian Centre for International Agricultural Research, 379–417.

González-García M, Almeida AC, Hevia A, Majada J, Beadle C. 2016. Application of a process-based model for predicting the productivity of *Eucalyptus nitens* bioenergy plantations in Spain. *GCB Bioenergy* **8**: 194–210.

Gromski PS, Xu Y, Kotze HL, Correa E, Ellis DI, Armitage EG, Turner ML, Goodacre R. 2014. Influence of missing values substitutes on multivariate analysis of metabolomics data. *Metabolites* **4**: 433–452.

Guo H, Wang Y, Wang L, Hu P, Wang Y, Jia Y, Zhang C, Zhang Y, Zhang Y, Wang C, et al. 2017. Expression of the MYB transcription factor gene BplMYB46 affects abiotic stress tolerance and secondary cell wall deposition in *Betula platyphylla*. *Plant Biotechnology Journal* **15**: 107–121.

Hacke UG, Sperry JS, Pockman WT, Davis SD, McCulloh KA. 2001. Trends in wood density and structure are linked to prevention of xylem implosion by negative pressure. *Oecologia* **126**: 457–461.

Hawkins E, Sutton R. 2012. Time of emergence of climate signals. *Geophysical Research Letters* **39**: 1–6.

Hertzberg M, Aspeborg H, Schrader J, Andersson A, Erlandsson R, Blomqvist K, Bhalerao R, Uhlén M, Teeri TT, Lundeberg J, et al. 2001. A transcriptional roadmap to wood formation. *Proceedings of the National*

Academy of Sciences of the United States of America **98**: 14732–14737.

Hinchee M, Rottmann W, Mullinax L, Zhang C, Chang S, Cunningham M, Pearson L, Nehra N. 2009. Short-rotation woody crops for bioenergy and biofuels applications. *In vitro cellular & developmental biology*. **45**: 619–629.

Hoffmann B, Münch S, Schwägele F, Neusüß C, Jira W. 2017. A sensitive HPLC-MS/MS screening method for the simultaneous detection of lupine, pea, and soy proteins in meat products. *Food Control* **71**: 200–209.

Hou Q, Ufer G, Bartels D. 2016. Lipid signalling in plant responses to abiotic stress. *Plant, Cell & Environment* **39**: 1029–1048.

Hussey SG, Mizrahi E, Creux NM, Myburg AA. 2013. Navigating the transcriptional roadmap regulating plant secondary cell wall deposition. *Frontiers in plant science* **4**: 1–21.

Hussey SG, Mizrahi E, Spokevicius A V, Bossinger G, Berger DK, Myburg A a. 2011. SND2, a NAC transcription factor gene, regulates genes involved in secondary cell wall development in *Arabidopsis* fibres and increases fibre cell area in *Eucalyptus*. *BMC plant biology* **11**: 173.

IPCC. 2013. Stocker, T.F., D. Qin, G.-K. Plattner, M. Tignor, S.K. Allen, J. Boschung, A. Nauels, Y. Xia, V. Bex and P.M. Midgley. *Climate Change 2013: The Physical Science Basis. Contribution of Working Group I to the Fifth Assessment Report of the Intergovernmental Panel on Climate Change*. Cambridge, UK & New York, NY, USA: Cambridge University Press, 1535 pp..

Jansen S, Gortan E, Lens F, Lo Gullo MA, Salleo S, Scholz A, Stein A, Trifilò P, Nardini A. 2011. Do quantitative vessel and pit characters account for ion-mediated changes in the hydraulic conductance of angiosperm xylem? *New Phytologist* **189**: 218–228.

Karabourniotis G, Liakopoulos G, Nikolopoulos D, Bresta P, Stavroulaki V, Sumbele S. 2014. “Carbon gain vs. water saving, growth vs. defence”: Two dilemmas with soluble phenolics as a joker. *Plant Science* **227**: 21–27.

Kim D, Pertea G, Trapnell C, Pimentel H, Kelley R, Salzberg SL. 2013. TopHat2: accurate alignment of transcriptomes in the presence of insertions, deletions and gene fusions. *Genome Biology* **14**: R36.

Kuhn AJ, Schröder WH, Bauch J. 1997. On the Distribution and Transport of Mineral Elements in Xylem, Cambium and Phloem of Spruce (*Picea abies* [L.] Karst.). *Holzforschung* **51**: 487–496.

Laclau J-P, Almeida JCR, Goncalves JLM, Saint-Andre L, Ventura M, Ranger J, Moreira RM, Nouvellon Y. 2009. Influence of nitrogen and potassium fertilization on leaf lifespan and allocation of above-ground growth in *Eucalyptus* plantations. *Tree Physiology* **29**: 111–124.

Langer K, Ache P, Geiger D, Stinzinger A, Arend M, Wind C, Regan S, Fromm J, Hedrich R. 2002. Poplar potassium transporters capable of controlling K⁺ homeostasis and K⁺-dependent xylogenesis. *The Plant journal : for cell and molecular biology* **32**: 997–1009.

Langer K, Levchenko V, Fromm J, Geiger D, Steinmeyer R, Lautner S, Ache P, Hedrich R. 2004. The poplar K⁺ channel KPT1 is associated with K⁺ uptake during stomatal opening and bud development. *The Plant journal : for cell and molecular biology* **37**: 828–838.

Langfelder P, Horvath S. 2008. WGCNA: an R package for weighted correlation network analysis. *BMC Bioinformatics* **9**: 559.

Lê Cao K-A, Costello M-E, Lakis VA, Bartolo F, Chua X-Y, Brazeilles R, Rondeau P. 2016. MixMC: A Multivariate Statistical Framework to Gain Insight into Microbial Communities (G Moreno-Hagelsieb, Ed.). *PLOS ONE* **11**: e0160169.

Legay S, Lacombe E, Goicoechea M, Brière C, Séguin A, Mackay J, Grima-Pettenati J. 2007. Molecular characterization of EgMYB1, a putative transcriptional repressor of the lignin biosynthetic pathway. *Plant Science* **173**: 542–549.

Li Z, Fernie AR, Persson S. 2016a. Transition of primary to secondary cell wall synthesis. *Science Bulletin* **61**: 838–846.

Li Z, Omranian N, Neumetzler L, ting Wang, Herter T, Usadel B, Demura T, Giavalisco P, Nikoloski Z, Persson S. 2016b. A Transcriptional and Metabolic Framework for Secondary Wall Formation in *Arabidopsis*. *Plant Physiology* **172**: pp.01100.2016.

Love MI, Huber W, Anders S. 2014. Moderated estimation of fold change and dispersion for RNA-seq data with DESeq2. *Genome Biology* **15**: 550.

Maere S, Heymans K, Kuiper M. 2005. BiNGO: a Cytoscape plugin to assess overrepresentation of Gene Ontology categories in Biological Networks. *Bioinformatics* **21**: 3448–3449.

Mansfield SD. 2009. Solutions for dissolution--engineering cell walls for deconstruction. *Current opinion in biotechnology* **20**: 286–94.

Mellerowicz EJ, Gorshkova TA. 2012. Tensional stress generation in gelatinous fibres: a review and possible mechanism based on cell-wall structure and composition. *Journal of Experimental Botany* **63**: 551–565.

Mitchell PJ, O’Grady AP, Hayes KR, Pinkard EA. 2014. Exposure of trees to drought-induced die-off is defined by a common climatic threshold across different vegetation types. *Ecology and evolution* **4**: 1088–1101.

Mitsuda N, Iwase A, Yamamoto H, Yoshida M, Seki M, Shinozaki K, Ohme-Takagi M. 2007. NAC

transcription factors, NST1 and NST3, are key regulators of the formation of secondary walls in woody tissues of *Arabidopsis*. *The Plant cell* **19**: 270–80.

Mizrachi E, Mansfield SD, Myburg AA. 2012. Cellulose factories: Advancing bioenergy production from forest trees. *New Phytologist* **194**: 54–62.

Mizrachi E, Verbeke L, Christie N, Fierro AC, Mansfield SD, Davis MF, Gjersing E, Tuskan GA, Van Montagu M, Van de Peer Y, et al. 2017. Network-based integration of systems genetics data reveals pathways associated with lignocellulosic biomass accumulation and processing. *Proceedings of the National Academy of Sciences* **114**: 1195–1200.

Nardini A, Grego F, Trifilo P, Salleo S. 2010. Changes of xylem sap ionic content and stem hydraulics in response to irradiance in *Laurus nobilis*. *Tree Physiology* **30**: 628–635.

Plasencia A, Soler M, Dupas A, Ladouce N, Silva-Martins G, Martinez Y, Lapierre C, Franche C, Truchet I, Grima-Pettenati J. 2016. *Eucalyptus* hairy roots, a fast, efficient and versatile tool to explore function and expression of genes involved in wood formation. *Plant Biotechnology Journal* **14**: 1381–1393.

Plomion C, Leprovost G, Stokes A. 2001. Wood Formation in Trees. *Plant Physiology* **127**: 1513–1523.

Ployet R, Soler M, Carocha V, Ladouce N, Alves A, Rodrigues J-C, Harvengt L, Marque C, Teulière C, Grima-Pettenati J, et al. 2018. Long cold exposure induces transcriptional and biochemical remodelling of xylem secondary cell wall in *Eucalyptus*. *Tree Physiology* **38**: 409–422.

Ramírez V, Agorio A, Coego A, García-Andrade J, Hernández MJ, Balaguer B, Ouwerkerk PBF, Zarra I, Vera P. 2011. MYB46 modulates disease susceptibility to *Botrytis cinerea* in *Arabidopsis*. *Plant physiology* **155**: 1920–1935.

Reimand J, Arak T, Adler P, Kolberg L, Reisberg S, Peterson H, Vilo J. 2016. g:Profiler—a web server for functional interpretation of gene lists. *Nucleic acids research* **44**: W83–9.

Sardans J, Peñuelas J. 2015. Potassium: a neglected nutrient in global change. *Global Ecology and Biogeography* **24**: 261–275.

Shi R, Wang JP, Lin Y-C, Li Q, Sun Y-H, Chen H, Sederoff RR, Chiang VL. 2017. Tissue and cell-type co-expression networks of transcription factors and wood component genes in *Populus trichocarpa*. *Planta* **245**: 927–938.

Singh A, Gautier B, Shannon CP, Vacher M, Rohart F, Tebutt SJ, Le Cao K-A. 2016. DIABLO - an integrative, multi-omics, multivariate method for multi-group classification. *bioRxiv*. <https://doi.org/10.1101/067611>

Smethurst P, Knowles A, Churchill K, Wilkinson A, Lyons A. 2007. Soil and foliar chemistry associated with potassium deficiency in *Pinus radiata*. *Canadian Journal of Forest Research* **37**: 1093–1105.

Soler M, Camargo ELO, Carocha V, Cassan-Wang H, San Clemente H, Savelli B, Hefer CA, Paiva JAP, Myburg AA, Grima-Pettenati J. 2015. The *Eucalyptus* grandis R2R3-MYB transcription factor family: Evidence for woody growth-related evolution and function. *New Phytologist* **206**: 1364–1377.

Stekhoven DJ, Buhlmann P. 2012. MissForest—non-parametric missing value imputation for mixed-type data. *Bioinformatics* **28**: 112–118.

Taylor-Teeples M, Lin L, Lucas M De, Turco G, Toal TW, Gaudinier A, Young NF, Trabucco GM, Lin L, de Lucas M, et al. 2015. An *Arabidopsis* gene regulatory network for secondary cell wall synthesis. *Nature* **517**: 571–575.

Trapnell C, Roberts A, Goff L, Pertea G, Kim D, Kelley DR, Pimentel H, Salzberg SL, Rinn JL, Pachter L. 2012. Differential gene and transcript expression analysis of RNA-seq experiments with TopHat and Cufflinks. *Nature Protocols* **7**: 562–578.

Van Acker R, Leplé J-C, Aerts D, Storme V, Goeminne G, Ivens B, Légée F, Lapierre C, Piens K, Van Montagu MCE, et al. 2014. Improved saccharification and ethanol yield from field-grown transgenic poplar deficient in cinnamoyl-CoA reductase. *Proceedings of the National Academy of Sciences of the United States of America* **111**: 845–50.

Van Acker R, Vanholme R, Piens K, Boerjan W. 2016. Saccharification protocol for small-scale lignocellulosic biomass samples to test processing of cellulose into glucose. In: *BIO-PROTOCOL* **6**(1): e1701.

Vanholme R, Storme V, Vanholme B, Sundin L, Christensen JH, Goeminne G, Halpin C, Rohde A, Morreel K, Boerjan W. 2012. A systems biology view of responses to lignin biosynthesis perturbations in *Arabidopsis*. *The Plant cell* **24**: 3506–29.

De Vos RCH, Moco S, Lommen A, Keurentjes JJB, Bino RJ, Hall RD. 2007. Untargeted large-scale plant metabolomics using liquid chromatography coupled to mass spectrometry. *Nature Protocols* **2**: 778–791.

Wang Y, Chantreau M, Sibout R, Hawkins S, Loqué D, Berkeley L, Wilkerson CG, State M. 2013. Plant cell wall lignification and monolignol metabolism. *Frontiers in Plant Science* **4**: 1–14.

Wang JP, Matthews ML, Williams CM, Shi R, Yang C, Tunlaya-Anukit S, Chen H-C, Li Q, Liu J, Lin C-Y, et al. 2018. Improving wood properties for wood utilization through multi-omics integration in lignin biosynthesis. *Nature Communications* **9**: 1579.

Wildhagen H, Paul S, Allwright M, Smith HK, Malinowska M, Schnabel SK, Paulo MJ, Cattonaro F, Vendramin V, Scalabrin S, *et al.* 2018. Genes and gene clusters related to genotype and drought-induced variation in saccharification potential, lignin content and wood anatomical traits in *Populus nigra*. *Tree Physiology* **38**: 320–339.

Wind C, Arend M, Fromm J. 2004. Potassium-Dependent Cambial Growth in Poplar. *Plant Biology* **6**: 30–37.

Wright SJ. 2011. The carbon sink in intact tropical forests. *Global Change Biology* **19**: 337–339.

Yamaguchi M, Ohtani M, Mitsuda N, Kubo M, Ohme-Takagi M, Fukuda H, Demura T. 2010. VND-INTERACTING2, a NAC domain transcription factor, negatively regulates xylem vessel formation in *Arabidopsis*. *The Plant cell* **22**: 1249–63.

Yang JH, Wang H. 2016. Molecular Mechanisms for Vascular Development and Secondary Cell Wall Formation. *Frontiers in Plant Science* **7**: 356.

Zhong R, Demura T, Ye Z-H. 2006. SND1, a NAC domain transcription factor, is a key regulator of secondary wall synthesis in fibers of *Arabidopsis*. *The Plant cell* **18**: 3158–70.

Zinkgraf M, Liu L, Groover A, Filkov V. 2017. Identifying gene coexpression networks underlying the dynamic regulation of wood-forming tissues in *Populus* under diverse environmental conditions. *New Phytologist* **214**: 1464–1478.

Zwieniecki MA, Secchi F. 2015. Threats to xylem hydraulic function of trees under ‘new climate normal’ conditions. *Plant, Cell & Environment* **38**: 1713–1724.

6. Figure legends

Figure 1: Water exclusion and K-fertilization induce changes in xylem transcriptome and metabolome. (a) and (b) Field picture of the four years old *Eucalyptus grandis* trees submitted to four treatments: [+W-K], [-W-K], [+W+K] and [-W+K]. In conditions [+W] and [-W], trees received respectively 100% and 63% of rainfall water (Battie-Laclau *et al.*, 2014b). In conditions +K and -K, trees were supplemented or not with K. (c) PLS-DA analyses of 5573 genes (DEGs) differentially expressed (fold change ≥ 2 or ≤ 0.5 and $P_{FDR} < 0.01$, $n = 3$) in response to water exclusion and K fertilization (**Table S1**). The first three principal components (PC) separates the four treatments and explain 82% of total variability. PC1 (61% of total variability) explains the separation between [+K] and [-K] treatments. PC2 and PC3 (respectively 12% and 8% of total variability) explain the separation between +W and -W treatments. Venn diagram describes the proportion of DEGs regulated by water exclusion (+W *versus* -W), potassium supply (+K *versus* -K) or both. (d) PLS-DA analyses of 516 mass signatures (DAMs) differentially accumulated ($P_{FDR} < 0.05$, $n=4$, peak intensity fold change ≥ 2 or ≤ 0.5) in response to water exclusion and K fertilization (**Table S2**). The first three principal components (PC) explain 76% of total variability and separate the four treatments. PC1 (39% of total variability) explains the separation between [+K] and [-K] treatments. PC2 and PC3 (21% and 16% of total variability respectively) explain the separation between [+W] and [-W] treatments. Venn diagram describes the proportion of DAMs regulated by water exclusion, potassium supply or both.

Figure 2: The changes in transcriptome occur in a broad range of biological processes.

Gene Ontology (GO) enrichment analysis on differentially expressed genes (DEGs), in response to K fertilization (5358 DEGs, 96%) or water exclusion (2151 DEGs, 38.5%), in *Eucalyptus grandis* trees. Network created from BiNGO (Maere *et al.*, 2005) results, manually reorganized and curated to remove non-informative GO terms. A total of 159 significantly enriched GO terms ($P_{\text{FDR}} < 0.01$) were kept. Node size is proportional to the number of genes found within GO categories. We made a hierarchical classification of these categories from the most general (level 1) to the most specialized level (level 9). Complete list of GO terms of levels 1 to 9 is provided in **Table S1**. The 45 level 9 GOs are linked to development (13 GOs), biotic and abiotic stress responses (4 and 10 GOs respectively), primary metabolism (7 GOs), biological regulation (4 GOs), cell wall biosynthesis (3 GOs), secondary metabolism (2 GOs) and transport (2 GOs). We represented in green dots the GOs enriched in DEGs regulated only by K (23 GOs), in blue dots the GOs enriched in DEGs regulated only by W (7 GOs) and in grey dots the GOs enriched in DEGs regulated by W&K (15 GOs).

Figure 3: Co-regulation network highlights modules of highly correlated genes involved in biological processes associated to cell wall formation.

Weighted co-expression network obtained by computing Pearson correlations between standardized profiles of 5,573 DEGs and 516 DAMs. Edge lengths are proportional to correlations. The network was visualized using Cytoscape software (force directed layout), it is composed of 170,629 significant correlations ($P_{\text{FDR}} < 5 \times 10^{-5}$) between 4,305 nodes. Grey and red edges represented positive and negative correlations respectively. Only 2,135 correlations were negative (**Table S3**). Two small isolated subnetworks (<10 variables) were not considered in the analyses. Twelve modules, detected by WGCNA analyses (Langfelder & Horvath, 2008), were represented by different node colors. For each module, gene expression profiles in the four treatments (**Table S1**) were represented by heatmaps. [+K], [-K], with and without potassium; [-W], [+W], with and without water exclusion respectively. We performed a Gene Ontology (GO) enrichment approach using functional annotation of the first BLAST hit of *Eucalyptus grandis* genes in *A. thaliana* genome (**Table S4**) to detect biological processes associated to DEGs enclosed in each module.

Figure 4: DAMs – Modules correlation network using MixOmics integrative approach.

(a) Network representing correlations (edges, >0.8) detected between DAMs, DEGs and the average profiles of the 12 modules. Modules profiles were calculated from the average expression profiles of DEGs within each module and we used the same color code as in Fig. 3. Diamond nodes represent mass signatures with size proportional to their connectivity. Poorly connected nodes were removed for graphical representation (connectivity < 3). Red diamonds represent DAMs selected for identification by LC-MS-MS (all connected to M1 to M6 modules). Edges are proportional to the absolute value of correlation (Table S3). DAMs – DAMs correlations were removed to improve graphical representation. DAMs accumulation profiles in the four treatments are represented by heat map. [+K], [-K], *Eucalyptus grandis* trees with and without potassium; [-W], [+W], *Eucalyptus grandis* trees with and without water exclusion. (b) Heat map representing accumulation profiles of the 14 identified DAMs. Most of them are negatively correlated to modules M1 to M6.

Figure 5: Cell wall related modules are correlated with wood phenotypic traits. Average stem biomass increment (Δ stem biomass), average gross primary productivity allocated to stem growth (GPP stem), saccharification yield, wood density, vessels size and vessel density were measured on developing xylem of *Eucalyptus grandis* trees submitted to potassium supply (+K and -K) and water exclusion (+W and -W). The phenotypic traits profiles are correlated to (i) the average profile of the 12 modules (Fig. 3) and (ii) 2,184 variables (36 DAMs and 2,148 DEGs) presenting the highest correlation values (<0.9) with at least one phenotypic traits ($P < 0.05$, Table S3). Edges (5,726) are proportional to the absolute value of correlations. Positive and negative correlations are represented respectively by solid lines and dash lines. DEGs, differentially expressed genes; DAMs, differentially accumulated metabolites. Dots color correspond to modules color according to Fig. 3. Letters represent significant differences between treatments (ANOVA HSD Tuckey test, $n=4$) and error bars represent \pm SD.

Figure 6: Transcription factors highly co-regulated with secondary cell wall biosynthesis in stress conditions. This subnetwork of 162 nodes was extracted from modules M1 to M6 (Fig. 3) and included significant correlations (edges, $P_{\text{FDR}} < 5.10^{-5}$) between 145 DEGs. In addition to DEGs - DEGs correlations we added the correlations with (1) the 14 identified DAMs (DEGs - DAMs correlations from MixOmics analyses, Fig. 4),

and (2) the correlations with saccharification yield, vessel density and vessel size (DEGs - phenotypic traits correlations from WGCNA analyses, **Fig. 5**). Among the DEGs, 113 were related to SCW formation: 97 were related to CW or SCW biosynthesis (22 related to cellulose, 56 to hemicelluloses, 19 to lignin, bottom panel) and 16 were putative orthologs of TFs involved in SCW formation (left panel). In the right panel, 32 uncharacterized TFs represent new candidates potentially involved in SCW remodeling. Only the most connected TFs (connectivity > 4) correlated to at least one phenotypic trait were kept (9 were not represented). They were all correlated positively to saccharification yield and vessel density, and negatively to vessel diameter and identified DAMs accumulation profiles. The edges connected to the best candidate *EgMYB137* (**Table S5**) were represented in bold. Node size is proportional to the degree of connectivity (**Fig. 3, Table S3**). Letters represent significant differences between treatments (ANOVA HSD Tuckey test, n=4) and error bars represent SD. Normalized DEGs and DAMs profiles are represented by heatmaps and graphs in the four treatments: [+K], [-K], *Eucalyptus grandis* trees with and without potassium; [-W], [+W], *Eucalyptus grandis* trees with and without water exclusion.

Figure 7: *EgMYB137* is involved in xylem formation in *Eucalyptus* roots. GUS expression driven by *EgMYB137* promoter was observed in the main root of *Eucalyptus grandis* transgenic lines, **(a)** in vascular tissues (*in vitro*, young root tip), **(b)** in xylem vessels (differentiation zone) and **(c)** in axial parenchyma cells surrounding the youngest vessels immediately below cambium (5 months old roots). Observations were made in brightfield on free-hand cut sections. White arrowheads represent vessels. Co, cortex, Cz, cambial zone, Ph, phloem; Xy, xylem. **(d)** Five months old *Eucalyptus* roots observed in epifluorescence. The highest auto-fluorescence intensity is observed in cell wall (CW) of vessels and axial parenchyma cells immediately below cambium (white arrowhead). **(e)** Bright field observations of semi thin section of 5 months old control root (empty vector) stained with toluidine blue. Cz, cambial zone; Xy, xylem. **(f)** Bright field observations of semi thin section of 5 months old *p35S:EgMYB137* roots, showing fibers CW thickness increase. **(g)** Changes in CW thickness of vessels and fibers in *p35S:EgMYB137* root xylem. Vessels SCW was significantly thinner in *p35S:EgMYB137* lines ($1.99 \pm 0.04 \mu\text{m}$) as compared to control lines ($2.07 \pm 0.06 \mu\text{m}$). Fibers SCW was significantly thicker in *p35S:EgMYB137* lines ($2.60 \pm 0.05 \mu\text{m}$) as compared to control lines ($2.29 \pm 0.04 \mu\text{m}$). ***, $P < 0.0001$ (Student's T test). **(h)** Decrease of vessel density in *p35S:EgMYB137* root xylem ($10.4 \pm 1.4 \text{ mm}^{-2}$) as compared to control ($16.1 \pm 3.1 \text{ mm}^{-2}$). *, $P < 0.05$ (Student's T test). Error bars represent SD (n=6 for

transgenic lines, n=4 for controls). Vessels CW thickness was measured on >70 vessels and >1200 fibers. Vessel density and lumen diameter were measured on >440 vessels and >1200 fibers. Scale bars, a, 200µm; b, 500µm; c-d, 150µm; e-f, 50µm.

Table 1: Over-expression of *EgMYB137* in *Eucalyptus grandis* roots changed saccharification yield

	<i>p35S::EgMYB137</i>	Control Ø
Saccharification yield without pretreatment (% of DW)	16.0 ± 1.8 *	19.1 ± 2.2
Saccharification yield with pretreatment (% of DW)	53.6 ± 5.8 **	63.6 ± 6.8

Analyses of saccharification yield was performed in triplicates for 9 lines of *p35S::EgMYB137* and 6 lines of controls (Ø, empty vectors). Values were significantly lower in *p35S::EgMYB137* lines compared to controls, in both pre-treated and non-pre-treated samples (± represents SD; *, $P < 0.05$; **, $P < 0.001$; Student's T test). Values are given as percentage of dry weight (DW) of extracted xylem residues (EXR).

7. Supporting information

Figure S1: Description of biological replicates and experimental methodology.

Figure S2: Monthly measurements of rainfall amount on experimental system from 2010 to 2018.

Figure S3: Principal Component Analyses (PCA) of metabolomic data illustrates the reproducibility of the 4 independent replicates.

Figure S4: Comparison of expression profiles obtained by RT-qPCR and RNAseq for a subset of selected genes

Figure S5: MixOmics network threshold selection.

Figure S6: Venn diagrams describing the effect of water availability and potassium supply on DEGs and DAMs repartition within each of the twelve modules detected by WGCNA analyses.

Figure S7: Heatmaps representing correlation values between average gene modules profiles and wood phenotypic traits.

Figure S8: Conservation of *EgMYB137* sub-network in *E. grandis*, *P. trichocarpa* and *A. Thaliana*.

Table S1: Transcriptomic data and gene ontology enrichment analyses.

Table S2: Metabolomic data analyses and DAMs identification.

Table S3: WGCNA networks construction and analyses.

Table S4: Expert annotation of DEGs related to SCW formation based on a comprehensive survey of the literature and a fine research of the closest orthologs in *Arabidopsis* genome.

Table S5: Identification of transcription factors (TFs) potentially involved in SCW remodeling in response to water exclusion and K-supply.

Methods S1: Biomass estimation, biochemical analyses, microscopy and histochemistry

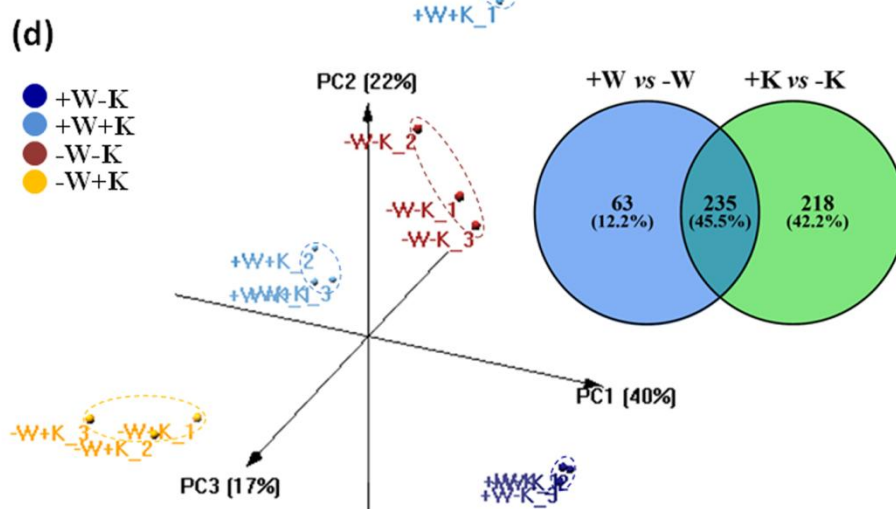
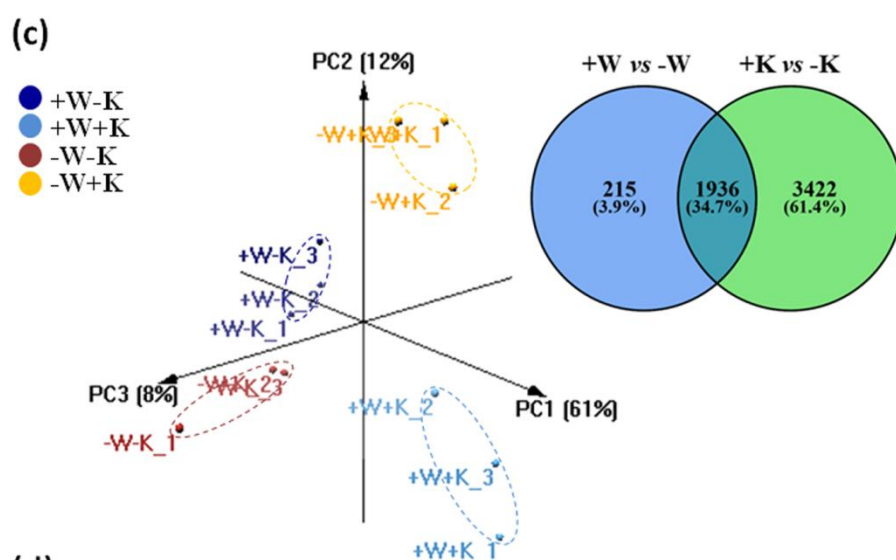
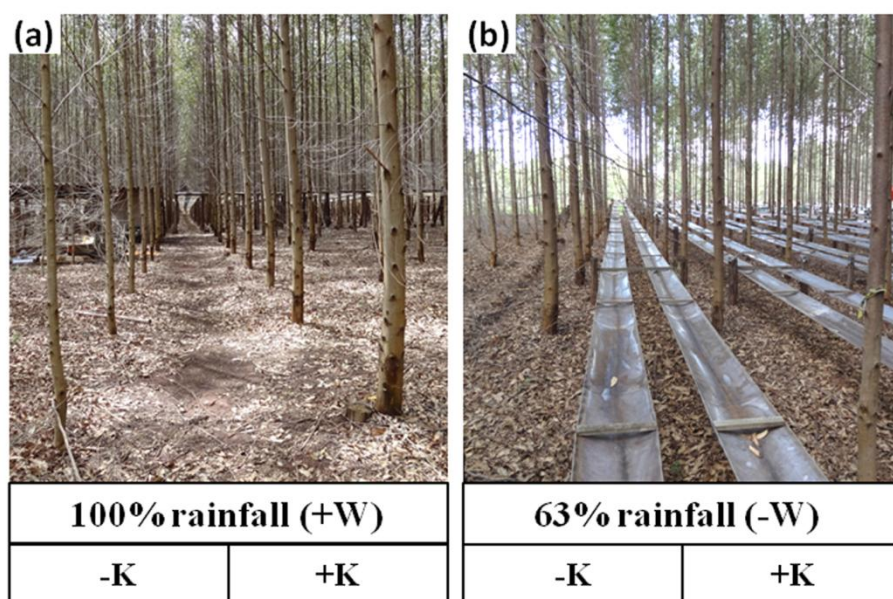
Methods S2: GC and LC-MS analyses

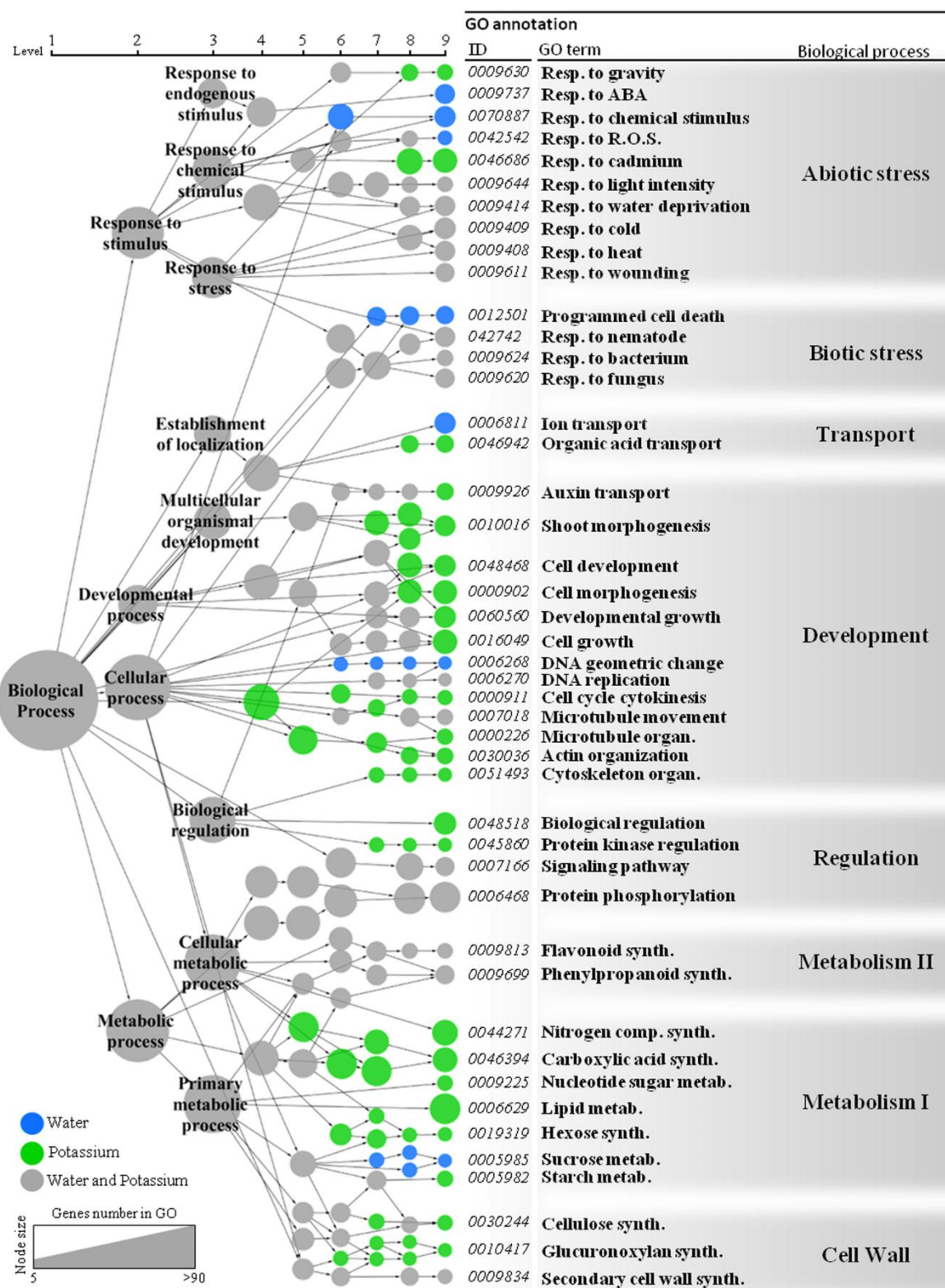
8. Acknowledgments

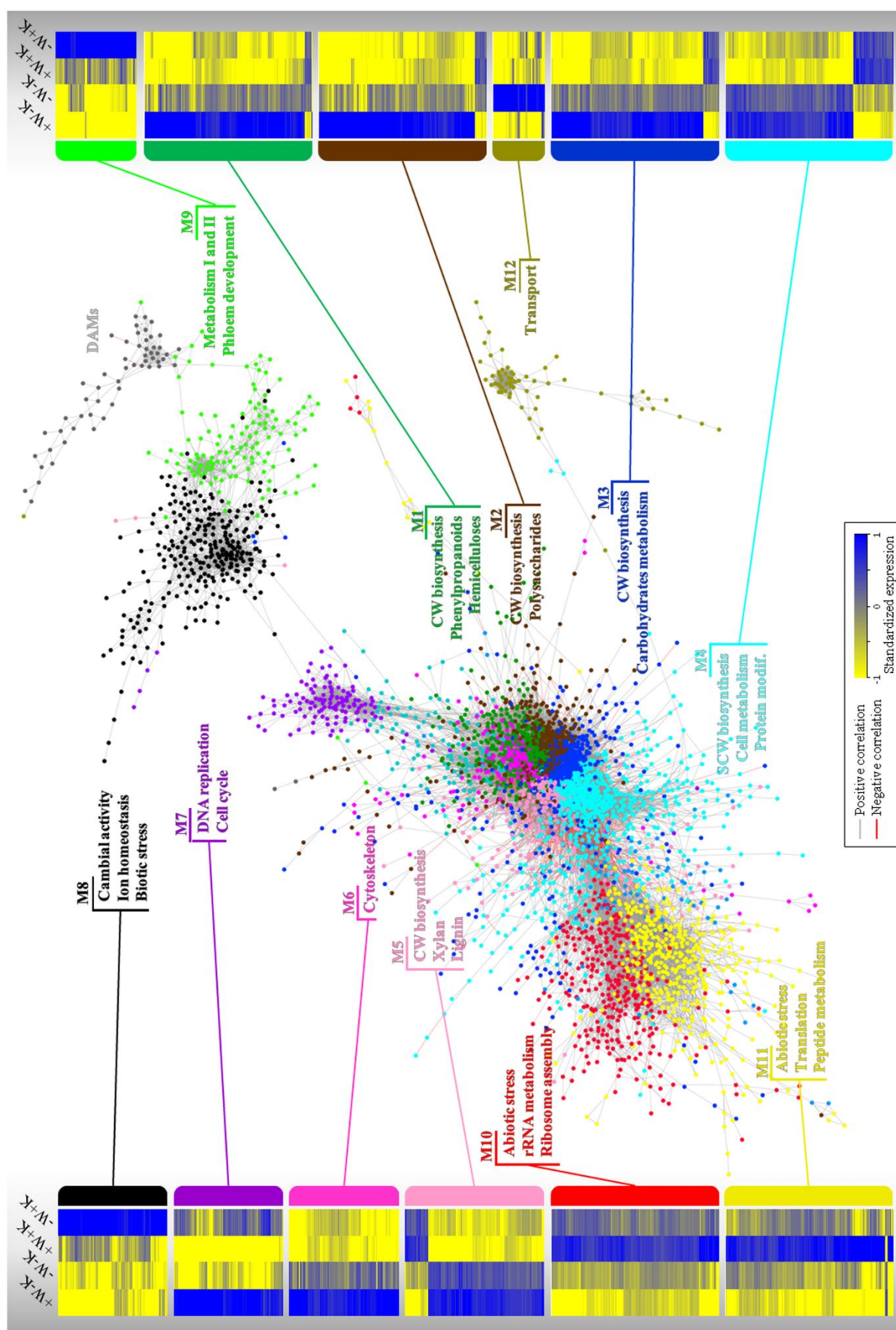
The experimental site belongs to the SOERE F-ORE-T, which is supported annually by Ecofor, Allenvi and the French National Research Infrastructure ANAEE-F (<http://www.anaee-france.fr/fr/>). This work was supported by the Centre National pour la Recherche Scientifique (CNRS), the French Laboratory of Excellence project ‘TULIP’ (ANR-10-LABX-41; ANR-11-IDEX-0002-02), Agropolis Fondation (project ID 1203-003, Investissements d’avenir programme, Labex Agro/ANR-10-LABX-372 0001-01) associated with CAPES (project: 017/13), CNPq (projects: 444793/2014-3 and 014/2012) and FAPESP (project 2013/25642-5). The authors acknowledge the University of Toulouse, the Genotoul GeT Platform, the TRI-Genotoul platform for microscopic analyses, M. Bermudez and A.C. Siqueira for their contribution in field trial. The authors acknowledge S. Déjean and K-A Lê Cao for their nice advices for the use of MixOmics. R.P. was supported by a PhD grant from the Ministère de l’Education Nationale, de l’Enseignement Supérieur et de la Recherche.

9. Author contribution:

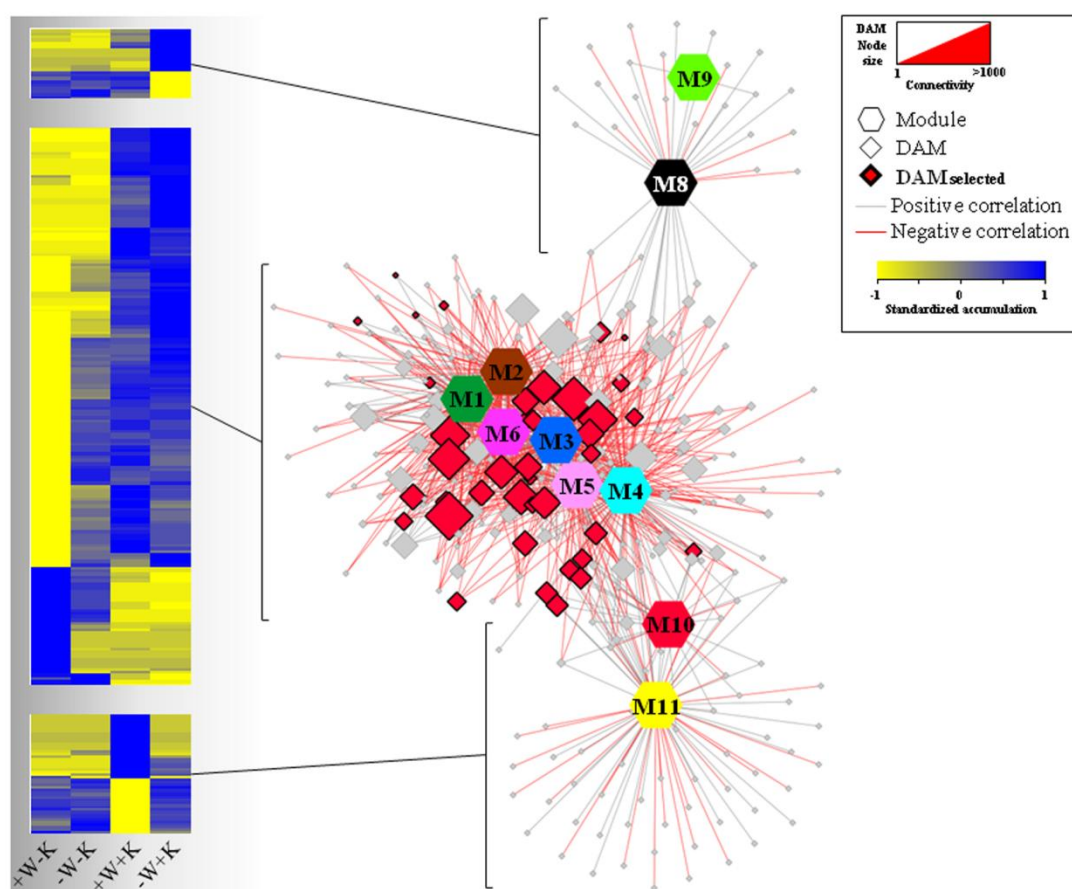
RP, MTVL, MC, BF, MTF, JPL, CAL, GC, JGP and FM contributed to manuscript redaction. RP, HSC, BF, MD, FM contributed to statistics, bioinformatic and data analyses. RP, GC performed xylem sampling. RP, MM, GC, FM, contributed to RNA extraction and wood phenotypic traits analyses. RP, MTVL, TRC, BF contributed to extraction and metabolomics analyses. RP, FM, MM contributed to transgenic plants characterization.







(a)



(b)

	+W-K	-W-K	+W+K	-W+K	ID	Name	Class
					pos_104	Octadecanamide	lipid
					neg_79	6-Hydroxyuteolin 6-xyloside	flavonoid
					neg_16	Xanthohumol C	flavonoid
					pos_92	Hydroxypropyl-Lysine	Amino acids derivative
					neg_171	10-Acetoxygustroside	terpenoid
					neg_249	2''-(6-Acetylglucosyl)astragalin	flavonoid
					pos_363	Phosphatidylethanolamine	lipid
					pos_346	Leucodelphinidin derivative	flavonoid
					pos_206	Kanzonol P	flavonoid
					pos_158	Perilloside A, Carveol glucoside	terpenoid
					pos_44	Trigoforin	coumarin
					pos_187	Acetylsalviposone	terpenoid
					pos_173	Neomenthol-glucuronide	terpenoid
					pos_393	Phosphatidylcholine	lipid

